Commensurability effects in hexagonal antidot lattices with large antidot diameters

S. Meckler and T. Heinzel*
Heinrich-Heine-Universität, Universitätsstr.1, 40225 Düsseldorf, Germany

A. Cavanna, G. Faini, U. Gennser, and D. Mailly
CNRS-LPN, Route de Nozay, 91960 Marcoussis, France
(Received 4 February 2005; published 11 July 2005)

The observation of a type of commensurability resonance in two-dimensional, hexagonal antidot lattices is reported. These resonances have a classical character and occur at magnetic fields above the resonance that corresponds to the cyclotron motion around a single antidot. The resonances are visible only for antidots with effective diameters larger than 50% of the lattice constant. Simulations reveal that they originate from quasistable electron trajectories that bounce between three neighboring antidots. This interpretation is backed by the observation of large-period Aharonov-Bohm-type oscillations at low temperatures.

DOI: 10.1103/PhysRevB.72.035319 PACS number(s): 73.23.−b, 73.63.−b

I. INTRODUCTION

The study of electron transport in artificial, two-dimensional periodic potentials has revealed a variety of interesting phenomena over the past 15 years. One variant of such systems is antidot lattices, i.e., periodic potentials with maxima above the Fermi energy of the two-dimensional electron gas (2DEG).[1–3] Most strikingly, resonances in the longitudinal magnetoresistance are found, which can be interpreted in terms of classical cyclotron orbits that are commensurate with the antidot lattice.[2] A more thorough classical treatment based on the Kubo formalism[4] has revealed that these resonances actually have their origin in the magnetic field dependent mixture of chaotic and regular trajectories, where the latter remain pinned in weak electric fields. Moreover, this theory provides an explanation for the observation of a negative Hall effect in weak magnetic fields B.[5] Another striking effect is the occurrence of B-periodic oscillations, which have been explained within a semiclassical theory by a few yet dominant quantized periodic orbits.[6,7] More recently, signatures of the famous fractal energy spectrum of such potentials, also known as the Hofstadter butterfly, have been observed.[8,9]

A large fraction of these studies was performed on square[1–3,6,8–10] or rectangular[11] lattices, while only a few experiments on hexagonal lattices have been published.[12–15] For the majority of the effects, the lattice type is, in principle, irrelevant. Nevertheless, hexagonal lattices show some peculiarities that are absent in other types of antidot lattices. In particular, Altshuler-Aronov-Spivak oscillations have been observed around $B=0$ in hexagonal lattices,[13,15] while Aharonov-Bohm oscillations can be detected at larger magnetic fields.[14,15] Also, it has been suggested recently that scattering centers with a short-range hexagonal order may be responsible for a phenomenology resembling the one observed in metal-insulator transitions in two dimensions.[16] Moreover, a detailed understanding of the transport in two-dimensional hexagonal lattices is of broad relevance, since this type of lattice forms via self-organization on a mesoscopic scale in a variety of systems, such as vortex lattices in type II superconductors[17] or diblock copolymers.[18]

Here, we report the observation of a novel type of magnetotransport resonance in hexagonal antidot lattices with large effective antidot diameters $d_e \geqslant 0.5a$, where a denotes the lattice constant. These resonances occur at cyclotron radii smaller than the antidot radius. Their signatures are visible only in the longitudinal component of the magnetoresistivity tensor, while temperature-dependent measurements indicate a classical origin. Furthermore, Aharonov-Bohm-type oscillations are observed at low temperatures that correspond to enclosed areas much smaller than the size of a lattice unit cell. These resonances are therefore attributed to quasistable trajectories that are localized *in between* three neighboring antidots. Numerical simulations of the magnetoresistivity based on the Kubo formalism support this interpretation and allow us to specify the characteristic trajectories.

The paper is organized as follows. In Sec. II, the sample preparation and the experimental setup are discussed. Section III is devoted to the experimental characterization of the resonances. In Sec. IV, we present numerical simulations, identify the relevant trajectories, and relate these results to the experiments. A summary and conclusion are given in Sec. V.

II. SAMPLE PREPARATION AND EXPERIMENTAL SETUP

Conventional modulation doped $GaAs/Al_{0.2}Ga_{0.8}As$ heterostructures with a two-dimensional electron gas (2DEG) 83 nm below the surface have been grown by molecular beam epitaxy. The 2DEG has an electron density of $n=2.5\times10^{15}$ m^{-2} and a carrier mobility of 90 m^2/Vs, corresponding to an elastic mean-free path of 7.6 μm and to a Drude scattering time of $\tau=35$ ps at liquid helium temperatures. A standard Hall bar geometry has been defined by optical lithography and wet chemical etching. The 2DEG is accessed electrically via Ni/AuGe Ohmic contacts. The hexagonal antidot arrays have been patterned by electron beam lithography and subsequent ion beam etching with low-energy (350 eV) Ar^+ ions.[19] The etch depth was 50 nm. All antidot arrays have a lattice constant of 600 nm, while lithographic antidot

diameters of d_l=100 nm, 200 nm, 250 nm, and 320 nm have been patterned. The measured array area was 50 μm $\times$25 μm.

Transport experiments have been carried out in a helium gas flow cryostat with a variable temperature insert and a superconducting magnet with a maximum field of B=8 T, which is applied perpendicular to the plane of the 2DEG. The temperature has been varied from 1.6 K to 24 K with an accuracy of 0.1 K. For measurements at lower temperatures, a top loading dilution refrigerator with a base temperature of 80 mK has been used. An ac current (frequency 33 Hz, amplitude 5 nA) was passed through the antidot array. The longitudinal (ρ_{xx}) and Hall (ρ_{xy}) components of the resistivity tensor have been determined from voltage differences measured in the corresponding four-probe setups.

III. EXPERIMENTAL RESULTS

Figure 1 shows the measurements of ρ_{xx} as a function of B for arrays with lithographic antidot diameters of d_l =100 nm, 200 nm, and 320 nm. Due to lateral depletion of the 2DEG around the antidots of about 100 nm, their electronic diameters d_e are larger. They can be estimated from the Shubnikov-de Haas oscillations observed in the antidot arrays, which give the Fermi wavelength in the array as well as, via their onset, the number of occupied transverse modes at the bottleneck formed by adjacent antidots. This way, effective electronic diameters of $d_e \approx$300 nm, 400 nm, and 550 nm, respectively, are found.

In the array with the smallest antidots [Fig. 1(a)], typical commensurability oscillations in ρ_{xx} are observed that, within the simple commensurability picture, in which the cyclotron diameter $r_c=m^* v_F/(eB)$ matches the lattice constant in the resistivity maxima, can be attributed to orbits around 1, 3, and 7 antidots.[12] Here, the resonance around one antidot occurs at B=270 mT. In comparison to the decay of the Shubnikov-de Haas oscillations with increasing temperature, the temperature dependence of the commensurability oscillations is weak, which indicates their classical origin. Note that there is an additional shoulder at B=200 mT and a peak at 70 mT with a weak temperature dependence [vertical arrows in Fig. 1(a)], which cannot be identified in this commensurability picture.

Figure 1(b) shows the corresponding measurements on a sample with d_l=200 nm. Here, only one strong resonance with a classical character is visible at B=130 mT, which, from simulations as described below, can be attributed to a superposition of the commensurability oscillations identified in Fig. 1(a). In addition, a weak resonance is observed at B =400 mT. It is clearly not related to the Shubnikov-de Haas oscillations that set in around B=0.6 T, and shows a weak temperature dependence. Such a structure is also present in an array with d_l=250 nm (not shown). Moreover, in Fig. 1(b), a small feature is observed between B=0.5 T and 0.7 T which, however, cannot be clearly distinguished from Shubnikov-de Haas oscillations. In arrays with even larger antidot diameters [Fig. 1(c)], three maxima, superimposed on a Shubnikov-de Haas resonance, are detected at $B \approx$0.45 T, 0.87 T, and 1.15 T. The main focus of the present paper is on the investigation of these resonances. The corresponding Hall measurements are shown in Fig. 2. While the structure of the conventional commensurability oscillations is reflected in $\rho_{xy}(B)$, no signatures of the novel resonances are detected here.

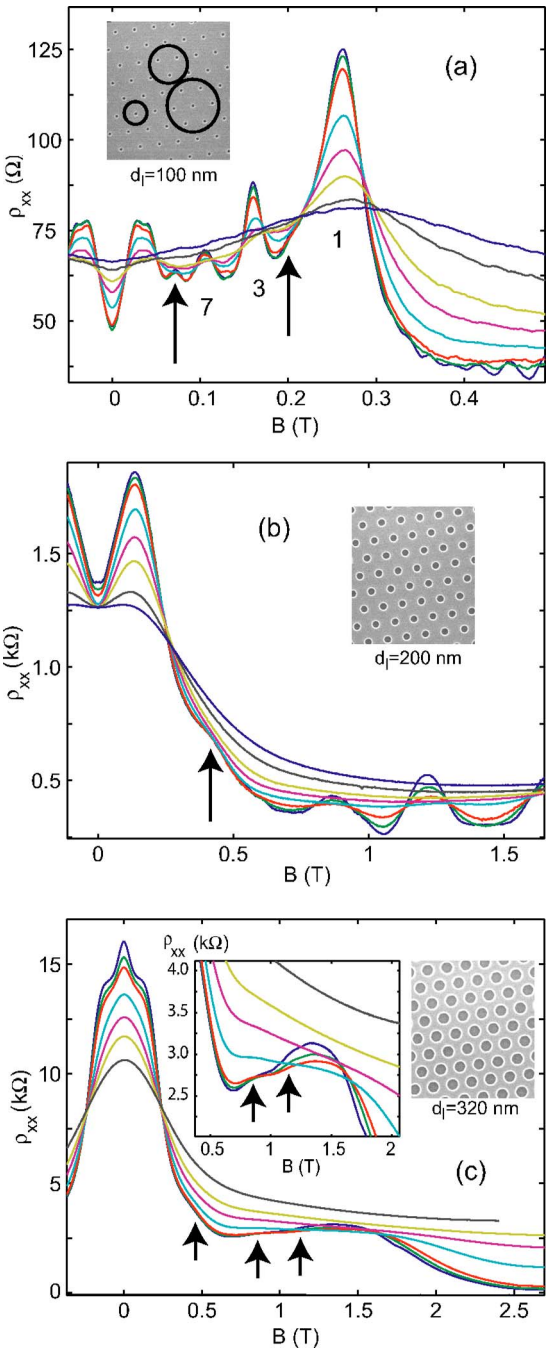

FIG. 1. (Color online) Longitudinal magnetoresistivity of the hexagonal antidot arrays at temperatures of T=1.5 K, 2.5 K, 4 K, 8 K, 12 K, 16 K, and 24 K, as observed for arrays with a=600 nm and different values of d_l (inset). In (a), the well-known resonances corresponding to cyclotron orbits around 1, 3, and 7 antidots are observed. In (b) and (c), a known resonance is observed around B =130 mT. The additional resonances are indicated by arrows. The inset in (c) shows a zoom in from the main figure of the region of interest.

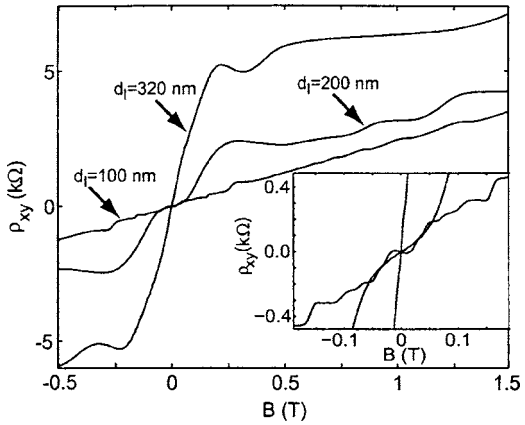

FIG. 2. Hall resistivities of the three arrays of Fig. 1, measured at $T=1.5$ K. In contrast to the conventional commensurability oscillations, the additional resonances cannot be identified. Note the negative Hall effect in the array with the small antidots (inset).

To obtain further insight into the character of these structures, we have studied the magnetotransport of the array with $d_l=320$ nm in a dilution refrigerator; see Fig. 3. Around $B=0$, the well-known Altshuler-Aronov-Spivak oscillations with a period of $\delta B=8$ mT are observed (not shown),[13] which evolve into quasiperiodic Aharonov-Bohm-type oscillations with a period of $\delta B=16$ mT for $B>60$ mT. The Aharonov-Bohm period corresponds to a characteristic area of $A=h/e\delta B=2.6\times10^{-13}$ m^2, in rough agreement with the area of a lattice unit cell ($A_{cell}=3.1\times10^{-13}$ m^2). This evolution has been reported and interpreted previously.[14] An additional, superimposed oscillation, however, with a period of $\delta B\approx120$ mT is observed in the magnetic field regime where the novel classical resonances are detected. Interpreting this oscillation in terms of an Aharonov-Bohm effect, the enclosed area equals $A\approx3.4\times10^{-14}$ m^2, which corresponds to about 11% of a unit cell. All periodic oscillations smear out as the temperature is increased, with the amplitude decaying roughly $\propto1/T$; the oscillation with the larger period persists to higher temperatures.

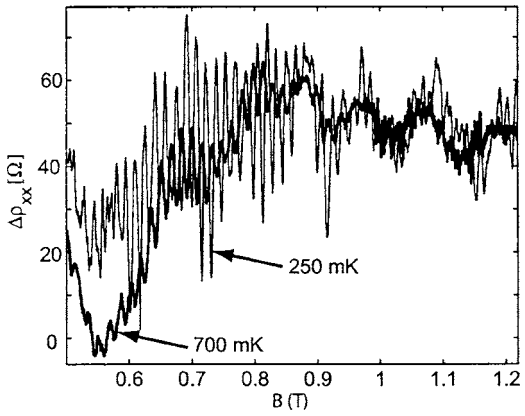

FIG. 3. Magnetoresistivity of the array with $d_l=320$ nm as measured in the dilution refrigerator in the magnetic field regime of the novel resonances. A smooth background has been subtracted. Here, the quasiperiodic Aharonov-Bohm oscillations are modulated with a period of $\delta B\approx120$ mT.

IV. INTERPRETATION AND DISCUSSION

We interpret our results in terms of commensurability oscillations that exist in the open electron pockets formed in between three adjacent antidots. Quasistable orbits may form by consecutive reflections of the electrons at the antidot walls. It seems plausible that such trajectories become more stable as d_e/a increases. We determine the characteristic area of such a pocket from $A_{pocket}=\frac{1}{2}[A_{cell}-\pi(d_e/2)^2]$ and estimate in our large antidot array to $A_{pocket}\approx3.6\times10^{-14}$ m^2, i.e., significantly smaller than the area of the unit cell. Hence, an increased Aharonov-Bohm period can be expected, although the exact period depends on the details of the closed trajectory.

In order to substantiate this interpretation, we have performed model calculations based on the Kubo formalism.[20] The antidot lattice is modeled by a two-dimensional, hexagonal array of hard-wall cylinders of the estimated electronic diameter d_e for the samples of Fig. 1. For each value of B, 10^5 electrons with a fixed Fermi energy adapted to the experimental conditions ($E_F=8.86$ meV) are injected at random positions and with random velocity directions within a unit cell of the lattice. Their trajectories are calculated to a length of 50 μm, corresponding to a time of flight of 240 ps. The electron velocity correlation function $\langle v_i(t,B)v_j(0)\rangle$ is calculated, where the brackets denote averaging over all trajectories.[21] Within the Kubo formalism, the components of the magnetoconductivity tensor for a degenerate two-dimensional electron gas are obtained from

$$\sigma_{ij}(B)=\frac{m^*e^2}{\pi\hbar^2}\int_0^\infty\langle v_i(t,B)v_j(0)\rangle e^{-t/\tau}dt \qquad (1)$$

In Eq. (1), $m^*=0.067m_e$ is the effective electron mass in GaAs. Elastic scattering due to random impurities is taken into account via the exponential cutoff function that appears in the integrand. Here, a Drude scattering time of $\tau=35$ ps has been chosen, in accordance with the mobility of the pristine 2DEG. This model is a simplified version of the more thorough treatment presented in Ref. 4. In particular, neither the driving electric field nor the finite slope of the antidot walls are taken into account. Nevertheless, our simplified model allows us to identify the trajectories that generate the additional resonances. In Fig. 4, the results of the simulated $\rho_{xx}(B)$ for the three arrays under study are reproduced. For the largest antidots ($d_e=550$ nm), pronounced resistivity minima are found around $B=0.78$ T, 1.4 T, and 1.85 T, while the commensurability resonance around a single antidot is barely visible at $B\approx0.3$ T.

To gain more insight into the origin of these structures, we have taken Poincaré sections along the perpendicular bisector of the line connecting the centers of two neighboring antidots; see Fig. 5. As the magnetic field increases to $B=0.6$ T, stable regions emerge with a structure as shown in Fig. 5(a). Around the resistivity maximum at 1 T, this pattern fades and evolves into a second one shown in Fig. 5(b), which is most pronounced around the minimum in ρ_{xx} at 1.4 T. As one goes to larger magnetic fields, the stable regions gradually fade until they can no longer be identified. We pick the Poincaré sections at $B=0.6$ T and 1.2 T for a detailed

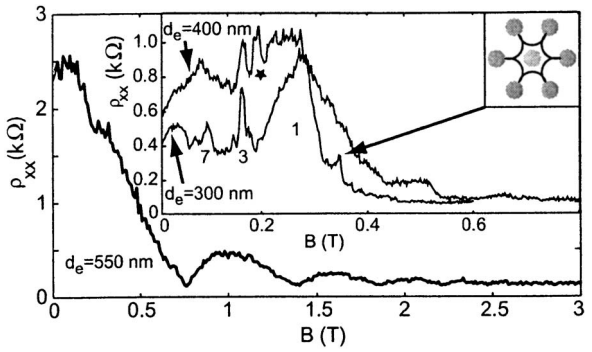

FIG. 4. Simulated longitudinal magnetoresistivity of the array with $d_e=550$ nm. Weak resonances are found in 0.6 T$\leqslant B\leqslant$2.2 T. The inset shows the corresponding simulations for the arrays with $d_e=300$ nm and $d_e=400$ nm. Here, the star denotes an unidentified resonance, while the cartoon to the upper right sketches the type of trajectory found in the feature indicated by the arrow.

discussion. In both cases, stable regions are found which contain the two types of trajectories shown in the right parts of Figs. 5(a) and 5(b), respectively. The first type is labeled by **1** and consists of skipping orbits around an individual antidot. This type is present for all magnetic fields above 0.5 T and covers a continuously increasing area in the Poincaré section as B is increased up to 2 T. Such skipping orbit trajectories have already been discussed for square antidot lattices.[10] The second type is triangularly or rosette-type shaped trajectories that form quasiclosed figures by consecutive reflections at walls of adjacent antidots. They are labeled by **2**–**4** in Fig. 5. The areas of the corresponding regular islands in the Poincaré sections have broad peaks, centered around the minima in ρ_{xx} at $B=0.78$ T and 1.4 T. Type 2 trajectories with two consecutive bounces at the same wall are present only for $B>1$ T. Hence, we attribute the structure in the resistivity of the array with the large antidots to the triangular or rosette-shaped trajectories. They are most important around the minima of ρ_{xx}, which is a consequence of the large magnetic field, since localized states that generate a minimum in $\sigma_{xx}(B)$ translate into a minimum in $\rho_{xx}(B)$ for $\rho_{xy}\gg\rho_{xx}$, as is the case here. Thus, a characteristic feature of the novel commensurability resonances that distinguishes them from those known previously is the fact that the magnetic field at which the quasistable trajectories are most pronounced corresponds to a minimum in ρ_{xx}.

Despite this qualitative agreement between the experimentally observed features and the simulations, quantitative differences are apparent. In particular, the positions of the measured minima and maxima in ρ_{xx} differ from the simulated ones, and their amplitudes are weaker, an effect that, due to the observed temperature independence, cannot be attributed to thermal smearing. Also, the structure stemming from rosette-type trajectories can be identified in simulations of the Hall resistivity (not shown), in contrast to our Hall measurements. One possible reason for these discrepancies may be nonspecular scattering at the antidot walls. Low-energy ion beam milling has been the technique of choice for patterning of the antidots, since it is established as a method to generate nanostructures with walls of high specularity

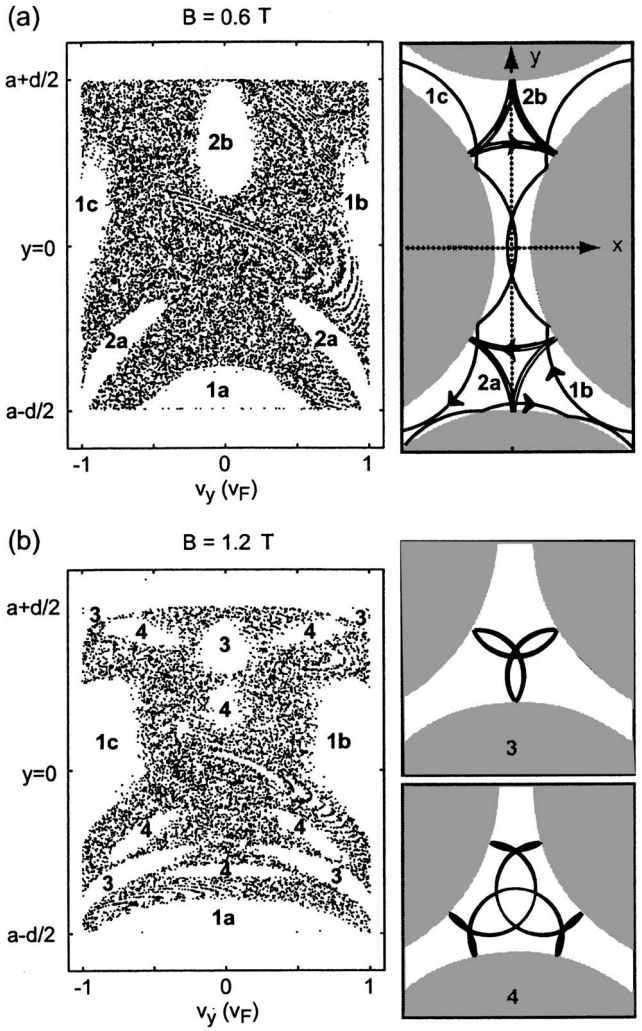

FIG. 5. Poincaré sections (left) taken from the array with $d_e=550$ nm at $B=0.6$ T (a) and 1.2 T (b). The sections are taken along the y direction at $x=0$; see the right part of (a), where the gray areas denote the antidots. The characteristic trajectories (right) found in the stable regions are assigned according to the numbers in the stable regions; see the text. Note that only the intersections of the trajectories with $v_x>0$ are plotted in the Poincaré sections.

around 85%.[19] We expect that the small fraction of nonspecular scattering may lead to some degree of smearing, but most likely not to a displacement of the extremal points. Rather, we interpret these deviations as a manifestation of soft antidot walls, probably in combination with some disorder in the antidot sizes, shapes, and positions, as well as the driving electric field. We are not aware of experimental work that determines the wall steepness for the etching technique we used. However, it seems plausible to assume that the steepness is comparable to that one obtained in Ga[Al]As samples of similar electron density, patterned by other dry etching techniques, like those used in Ref. 2. More elaborate simulations that use the wall steepness as a parameter[4,5] have been able to establish a close to perfect agreement with the experimental observations of Ref. 2. As an example, we note that a peak is observed in the experiments on antidot arrays with small diameters at small magnetic fields [Fig. 1(a)],

which cannot be attributed to a trajectory by our simulations. A similar discrepancy in square lattices[2] could be resolved by the softness of the walls,[4] a fact that suggests that the deviations in our study can be explained by soft walls as well. In general, soft walls tend to deform the trajectories, which in turn causes some resonances to be significantly displaced, while the sensitivity to the wall steepness depends on the resonance.[4] Such a deformation would be in tune with the observation that the areas enclosed by the simulated trajectories (Fig. 5) are smaller than the measured enclosed areas (Fig. 3). Also, the peak around 0.35 T in the simulated array with $d_e=300$ nm can be identified in a Poincaré section of the hard wall simulation (inset in Fig. 4), but is not observed experimentally. It seems plausible to us that such a trajectory is very sensitive to an even moderate softening of the wall. To find out whether more realistic simulations, or experiments on samples with steeper walls,[10] are able to resolve the discrepancies, is beyond the present study.

For the sample with the smallest antidot diameter, the simulations reproduce the experiments remarkably well in the range $r_c \geqslant a$ [Figs. 1(a), 2, and 4]. The measured negative Hall effect (Fig. 2) is reproduced in our hard wall simulations (not shown), in contrast to hard wall simulations performed for square lattices.[5] In square lattices consisting of antidots with similar ratios d/a, simulations do not suggest the existence of type 2 orbits, independent of the wall steepness.[10] Thus, the wall steepness seems less critical in hexagonal arrays, but becomes more relevant as d_e/a increases. We therefore conclude that a hexagonal lattice strongly favors the formation of stable orbits in between antidots as compared to square lattices.

V. SUMMARY AND CONCLUSION

In summary, we observe resonances in hexagonal antidot lattices with large antidot diameters. Classical simulations suggest that they can be attributed to classical, quasiperiodic trajectories of various shapes that are caught in between three adjacent antidots. This interpretation is supported by measurements at temperatures below 1 K, where the samples show Aharonov-Bohm-type oscillations with a characteristic area similar to that one of an electron pocket in between antidots. It remains to be seen whether such resonances are also visible in other types of antidot lattices with optimized parameters. In order to improve the quantitative agreement with simulations, it would be interesting to perform more sophisticated calculations with realistic potential landscapes, inclusion of the driving electric field, disorder, and the wave nature of the electrons.

ACKNOWLEDGMENTS

Financial support by the Heinrich-Heine-Universität Düsseldorf and by the Region Ile de France and the Conseil Général de l'Essonne is gratefully acknowledged. The authors acknowledge technical support by Ch. Dupuis.

*Electronic address: thomas.heinzel@uni-duesseldorf.de

[1] K. Ensslin and P. M. Petroff, Phys. Rev. B **41**, R12307 (1990).
[2] D. Weiss, M. L. Roukes, A. Menschig, P. Grambow, K. von Klitzing, and G. Weimann, Phys. Rev. Lett. **66**, 2790 (1991).
[3] A. Lorke, J. P. Kotthaus, and K. Ploog, Phys. Rev. B **44**, R3447 (1991).
[4] R. Fleischmann, T. Geisel, and R. Ketzmerick, Phys. Rev. Lett. **68**, 1367 (1992).
[5] R. Fleischmann, T. Geisel, and R. Ketzmerick, Europhys. Lett. **25**, 219 (1994).
[6] D. Weiss, K. Richter, A. Menschig, R. Bergmann, H. Schweizer, K. v. Klitzing, and G. Weimann, Phys. Rev. Lett. **70**, 4118 (1993).
[7] K. Richter, Europhys. Lett. **29**, 7 (1995).
[8] C. Albrecht, J. H. Smet, K. von Klitzing, D. Weiss, V. Umansky, and H. Schweizer, Phys. Rev. Lett. **86**, 147 (2001).
[9] T. Schlösser, K. Ensslin, J. P. Kotthaus, and M. Holland, Europhys. Lett. **33**, 683 (1996).
[10] J. Eroms, M. Zitzlsperger, D. Weiss, J. H. Smet, C. Albrecht, R. Fleischmann, M. Behet, J. DeBoeck, and G. Borghs, Phys. Rev. B **59**, R7829 (1999).
[11] R. Schuster, K. Ensslin, J. P. Kotthaus, M. Holland, and C. Stanley, Phys. Rev. B **47**, 6843 (1993).
[12] D. Weiss, K. Richter, E. Vasiadou, and G. Lütjering, Surf. Sci. **305**, 408 (1994).
[13] F. Nihey, S. W. Hwang, and K. Nakamura, Phys. Rev. B **51**, 4649 (1995).
[14] M. Ueki, A. Endo, S. Katsumoto, and Y. Iye, Photonics Spectra **22**, 365 (2004).
[15] Y. Iye, M. Ueki, A. Endo, and S. Katsumoto, J. Phys. Soc. Jpn. **73**, 3370 (2004).
[16] T. Heinzel, R. Jäggi, E. Ribeiro, M. v. Waldkirch, K. Ensslin, S. Ulloa, G. Medeiros-Ribeiro, and P. M. Petroff, Europhys. Lett. **61**, 674 (2003).
[17] M. Tinkham, *Introduction to Superconductivity* (Dover, New York, 2004).
[18] T. Thurn-Albrecht, J. Schotter, G. Kastle, N. Emley, T. Shibauchi, L. Krusin-Elbaum, K. Huarini, C. T. Black, M. T. Touminen, and T. P. Russell, Science **290**, 2126 (2000).
[19] Y. Lee, G. Faini, and D. Mailly, Phys. Rev. B **56**, 9805 (1997).
[20] R. Kubo, J. Phys. Soc. Jpn. **12**, 570 (1957).
[21] K. Richter, *Semiclassical Theory of Mesoscopic Quantum Systems* (Springer-Verlag, New York, 2004).